Dynamic Bayesian Network Modeling of Vascularization in Engineered Tissues

Caner Komurlu
Computer Science Department
Illinois Institute of Technology
Chicago, IL, 60616
ckomurlu@hawk.iit.edu

Jinjian Shao
Computer Science Department
Illinois Institute of Technology
Chicago, IL, 60616
jshao3@hawk.iit.edu

Mustafa Bilgic
Computer Science Department
Illinois Institute of Technology
Chicago, IL, 60616
mbilgic@iit.edu

Abstract

In this paper, we present a dynamic Bayesian network (DBN) approach to modeling vascularization in engineered tissues. Injuries and diseases can cause significant tissue loss to the degree where the body is unable to heal itself. Tissue engineering aims to replace the lost tissue through use of stem cells and biomaterials. For tissue cells to multiply and migrate, they need to be close to blood vessels, and hence proper vascularization of the tissue is an essential component of the engineering process. We model vascularization through a DBN whose structure and parameters are elicited from experts. The DBN provides spatial and temporal probabilistic reasoning, enabling tissue engineers to test sensitivity of vascularization to various factors and gain useful insights into the vascularization process. We present initial results in this paper and then discuss a number of future research problems and challenges.

1 INTRODUCTION

People lose tissue due to accidents, medical operations, treatments, and illnesses. While some organs, e.g. liver, can replace the lost tissue most cannot especially when the damage is too severe. For these kinds of tissue damages, the lost tissue can be replaced by engineering a new tissue through stem cells and biomaterials [18].

An essential process for engineering a healthy tissue is the proper vascularization (formation of new blood vessels) of the tissue, as the tissue cells need to be close to the blood vessels both to discharge their waste and to receive nutrition and oxygen. The blood vessels need to spread out in the tissue, invade into the depths of the tissue, and form connections to allow blood circulation.

The formation of new blood vessels are triggered and affected by growth factors that are released by distressed cells that are far from the existing blood vessels. When these growth factors reach existing blood vessels, they sprout new branches and these branches "search" for the distressed cells by following the gradient of the growth factor. This process, however, is stochastic for at least two reasons: i) even though growth factors are the main ingredients for causing sprouts, they are not the only elements that affect vascularization, and ii) the growth factors are increasingly more uniformly distributed as they go further away from the distressed cells, and hence the gradient is almost uniform, hindering the capability of the blood vessel finding its way correctly.

This inherent stochasticity in the vascularization process, the spatial nature of the tissue, and the temporal aspect of the vascularization make temporal graphical models a great fit for reasoning with uncertainty in vascularization. In this paper, we present a dynamic Bayesian network (DBN) for modeling vascularization in engineered tissues. We elicit the structure of the DBN from tissue engineering experts and we experiment with various parameter settings to provide further insights into the vascularization process. Because this is a first and novel application of DBNs to tissue engineering, it avails itself to many interesting future research directions and challenges.

Our contributions in this paper include:

- We present a novel application of DBNs to vascularization in engineered tissues
- We present initial results and insights, where we experiment with various parameter settings, and
- We discuss several future research challenges and opportunities in detail.

The rest of the paper is organized as follows: in Section 2, we provide a brief background on tissue engineering and vascularization. In Section 3, we describe our DBN model for vascularization. We present our experimental setup and results in Section 4. In Section 5, we briefly discuss related work. We then discuss future research directions and challenges in detail in Section 6, and then conclude.

2 BACKGROUND

In this section, we first provide a brief background on tissue engineering and vascularization and then discuss briefly why dynamic Bayesian networks (DBNs) are a good fit for modeling vascularization.

People lose tissue due to accidents, treatments, and illnesses. Some organs, e.g. liver, can replace the lost tissue while others cannot. Sometimes, the damage can be so severe that the body cannot heal itself. For example, bones can heal after smooth fractures. Yet, some fractures damage bone body so severely that the bone cannot regenerate. For these kinds of damages, the lost tissue can be replaced by engineering a new tissue through stem cells and biomaterials.

Stem cells are generic types of cells that have the ability to replicate and transform to any tissue. Stem cells, like all other cells, need to be close enough to the blood vessels so that they can forward their biological wastes to the vessels and they can be fed with nutrition and oxygen carried by the blood vessels. When a tissue is engineered through replication and transformation of stem and tissue cells, there is no existing blood vessel web in the environment; the only blood vessels available are the original vessels located at the edges, ready to sprout and progress to the depths of the newly-formed tissue.

The stem cells that do not have access to blood vessels will not be able to discharge waste and receive nutrition and oxygen. In such cases, a cell starts signaling about its needs by means of emitting chemicals called vascular endothelial growth factor (VEGF). VEGF diffuses and disperses in the environment. When it contacts a blood vessel, it triggers a new sprout of blood vessel towards the source of emission. The tip of these new sprouts typically follow the gradient of the VEGF to find the distressed cell. During this process, the newly-formed blood vessel can also branch and sprout new blood vessels. When the branches meet with other branches, they merge (this process is called anastomosis) and a blood circulation through the new vessel starts. The blood circulation helps nearby stem and tissue cells, which then stop emitting growth factors. This event is called angiogenesis or vascularization. Please see Figure 1 for an illustration of this process.

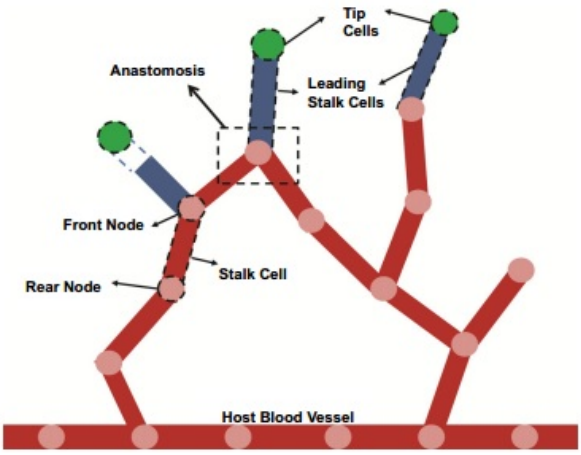

Figure 1: Illustration of vascularization, including the tip cells (active cells), the fixed cells (stalk cells), and anastomosis. [19]

Vascularization is a key process in tissue development. When cells that are emitting VEGF cannot be reached in time by the new blood vessels, the cells first fall in hypoxia (i.e., lack of Oxygen) and then start dying. Hence the formation of healthy tissue depends on appropriate vascularization; the blood vessels need to spread out in the newly-formed tissue, invade into the depth, and need to form connections to allow blood circulation.

Though it is well-known that the VEGF is a major contributor to sprouting of new blood vessels and that the tip of the blood vessel typically follows the gradient of the VEGF, there are still unknown factors that affect vascularization. Moreover, the VEGF distribution becomes more uniform as we get further away from the source of the emission and hence the gradient does not necessarily point to the distressed cell. Therefore, given our knowledge of the VEGF distribution the environment, the blood vessels do not necessarily follow a deterministic path; they also do a bit of exploration. This is where the uncertainty reasoning capabilities of probabilistic graphical models become handy for modeling vascularization.

In this paper, we model the vascularization process through dynamic Bayesian networks (DBNs) to enable tissue engineering researchers to reason with spatial and temporal growth of blood vessels. With the help of DBNs, the researchers can formulate and query the DBNs and try a number of parameter settings, without the need to experiment with every one of them in the lab. This process allows the researchers to gain further insights and formulate new in-vivo (on animals) and in-vitro (on glass) experiments.

3 APPROACH

In this section, we describe our DBN model for vascularization. We made a number of assumptions to simplify the model. In this model, we assume a 2D structure, whereas in real-life scenarios, the tissue obviously has a 3D structure. In this 2D structure, which is illustrated in Figure 2, as also assumed in [1], we assume that the blood vessel grows bottom-up towards north. Therefore, the status of a location at time t depends on: i) its status at time t, and ii) the statuses of its south neighbors at t.

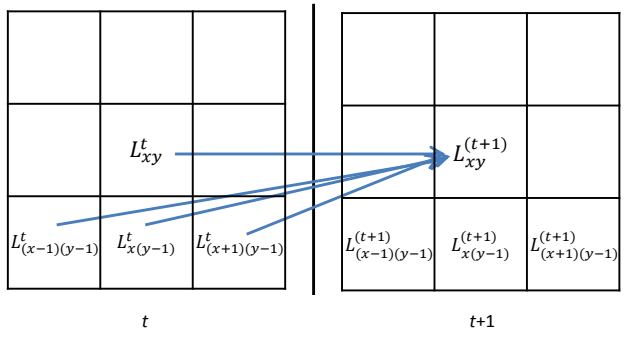

Figure 2: The tissue grid. Each cell of the grid represents a location, which can be `Empty`, or can be occupied with an `Active Cell` or `Stalk Cell`. Each location is represented as a random variable in DBN.

To simplify the notation, when we refer to a generic location L^t_{xy}, we will drop the subscripts and hence simply use L^t, and when we refer to its neighbors at its south $L^t_{(x-1)(y-1)}$, $L^t_{x(y-1)}$, and $L^t_{(x+1)(y-1)}$ we will simply use L^t_{SW}, L^t_S, and L^t_{SE}, corresponding to neighbors at south west, south, and south east, respectively. We illustrate the relevant 2-time slice dynamic Bayesian network in Figure 3.

Each location on the 2D grid is a random variable, representing whether that location is `Empty`, or occupied by a blood vessel cell. Blood vessel cells are two types: the tip of a blood vessel that has the potential to grow (henceforth called an `Active Cell`) or the body of the blood vessel (henceforth called the `Stalk Cell`). Therefore, the domain of random variable is [`Active Cell`, `Stalk Cell`, `Empty`], abbreviated henceforth as [AC, SC, E].

We model the conditional probability distribution, (CPD), $P\left(L^{(t+1)}|L^t, L^t_{SW}, L^t_S, L^t_{SE}\right)$ as a tree CPD as illustrated in Figure 4. To give a simple overview, at each step in time, an `Active Cell` elongates and moves into a nearby `Empty` location, forming the body of the blood vessel (i.e., `Stalk Cell`) in the process. The transitions are:

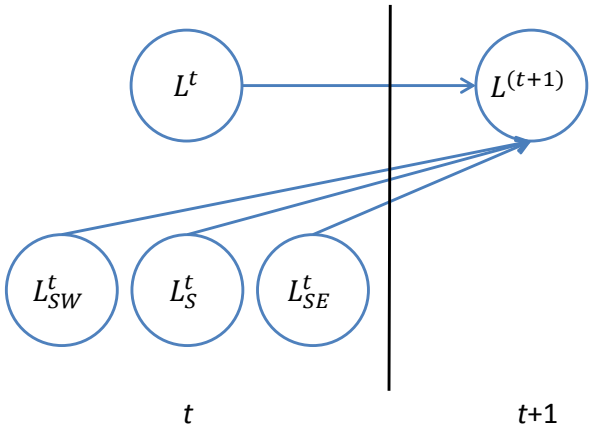

Figure 3: A two-time slice representation of the DBN. A location at a time $t+1$ has four parents: itself at time t and its lower neighbors at time t.

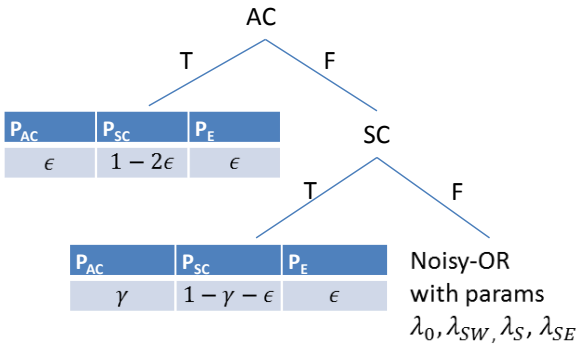

Figure 4: The CPD for $P(L^{(t+1)}|L^t, L^t_{SW}, L^t_S, L^t_{SE})$.

- The tip of a blood vessel (AC) at time t becomes the body (SC) at time $t+1$. That is $P\left(L^{(t+1)}|L^t = AC, L^t_{SW}, L^t_S, L^t_{SE}\right) = P\left(L^{(t+1)}|L^t = AC\right) = \langle \epsilon, 1-2\epsilon, \epsilon \rangle$, where ϵ is a small noise parameter.

- A `Stalk Cell` at time t either continues to remain a `Stalk Cell` at time $t+1$ or it might become `Active Cell` with probability γ to sprout a new blood vessel branch. That is, $P\left(L^{(t+1)}|L^t = SC, L^t_{SW}, L^t_S, L^t_{SE}\right) = P\left(L^{(t+1)}|L^t = SC\right) = \langle \gamma, 1-\gamma-\epsilon, \epsilon \rangle$. We refer to γ as the sprout possibility.

- An `Empty` location at time t will remain `Empty` at time $t+1$ if none of its SW, S, or SE neighbors are `Active Cell` at time t; if there is an `Active Cell` at one or more of those neighboring locations at time t, one of them might elongate to this `Empty` location at time $t+1$. The

probability of that an `Empty` location being occupied by an `Active Cell` at time $t+1$ is modeled as a Noisy-OR of its neighboring locations. That is $P\left(L^{(t+1)} = AC | L^t = E, L^t_{SW}, L^t_S, L^t_{SE}\right)$ is a Noisy-OR of $L^t_{SW}, L^t_S, L^t_{SE}$, with parameters λ_0, λ_{SW}, λ_S, and λ_{SE}, where λ_0 is leak parameter, and λ_{SW}, λ_S, and λ_{SE} corresponds to the possibility that an `Active Cell` elongates in the NE, N, or NW direction.[1] The magnitude of λ_{SW}, λ_S, and λ_{SE} are determined by the VEGF gradient. We refer to various configurations of the λ parameters as the growth patterns.

4 EXPERIMENTAL SETUP, RESULTS, AND INSIGHTS

In this section, we describe the experiments we performed using various settings for the growth pattern (λ) and sprout (γ) parameters. In all the experiments to follow, we set the noise ϵ and the leak λ_0 parameters to 0.01. For the growth pattern, we present results for two settings:

- `straight-growth`: $\langle \lambda_{SW}, \lambda_S, \lambda_{SE} \rangle = \langle 0.01, 0.98, 0.01 \rangle$. For this pattern, the blood vessel follows a straight line, growing towards north.
- `uniform-growth`: $\langle \lambda_{SW}, \lambda_S, \lambda_{SE} \rangle = \langle \frac{1}{3}, \frac{1}{3}, \frac{1}{3} \rangle$. For this pattern, the blood vessel has equal chance of growing towards north, north west, or north east.

For the sprout possibility, that is a `Stalk Cell` turning into an `Active Cell`, we present results for two settings:

- `seldom-sprout`: $\gamma = 0.01$. For this setting, the `Stalk Cell` has very small chance (probability of 0.01) of becoming an `Active Cell` in the next time step.
- `always-sprout`: $\gamma = 0.98$. For this setting, the `Stalk Cell` has 0.98 probability of becoming active in the next step. This is quite an unrealistic setting; we present it only for didactic purposes.

We present results for four possible configurations: the cross-product of the growth patterns and sprout possibilities. We first provide detailed results on a 3×3 grid over three time slices. Then, we present results on a bit larger scale, 9×9, over nine time slices. Finally, we present a framework where we quantify the uncertainty over the predictions on the last time slice and discuss how it is affected by the growth patterns and sprout possibilities.

For inference, in the 3×3 case, we used exact inference. For the 9×9 case, we used forward sampling. Note that we are able to use forward sampling in our settings because we provide the initial condition (all locations at time $t = 0$) as evidence and compute probabilities for the remaining time slices.

4.1 Detailed Results for 3×3

In this toy setting, we provide the evidence for the initial configuration of the experiment, i.e., we provide evidence for all locations for time $t = 0$, and compute probabilities for all locations for all future time slices. That is, we compute $P(\mathcal{L}^1, \mathcal{L}^2 | \mathcal{L}^0)$, where $\mathcal{L}^t$ denotes *all* locations at time t. For $t = 0$, we provide the evidence as follows: the middle of the bottom row is set as the tip of the blood vessel (i.e, $L^0_{x=1,y=0} = AC$) and the rest of the locations are set as `Empty`. Figure 5 illustrates this setting.

E	E	E
E	E	E
E	AC	E

Figure 5: The initial configuration for the 3×3 grid.

The `straight-growth` results are presented in Figures 6 and 7, and `uniform-growth` results are presented in Figures 8 and 9.

The simplest setting where the blood vessel grows in a straight path and that does not sprout at all (Figure 6) is fairly straightforward to analyze. The tip of the blood vessel migrates one location towards north at each step, forming the body of the vessel along the process. This setting, therefore, serves as a sanity check.

In the next setting, which is presented in Figure 7, we keep the growth pattern the same (`straight-growth`) but increase the sprout possibility to 0.98 (`always-sprout`). In this setting, the blood vessel grows towards north as expected. Unlike the `seldom-sprout` case, however, a `Stalk Cell` at time $t = 1$ became active at time $t = 2$.

Next, we present results for the `uniform-growth` cases. In this setting, the blood vessel has uniform

[1] Note that λ_{SW} denotes the probability that an `Active Cell` at the SW of an `Empty` location will move to this `Empty` location; hence λ_{SW} denotes the possibility that an `Active Cell` at SW moves in the NE direction to occupy an `Empty` location.

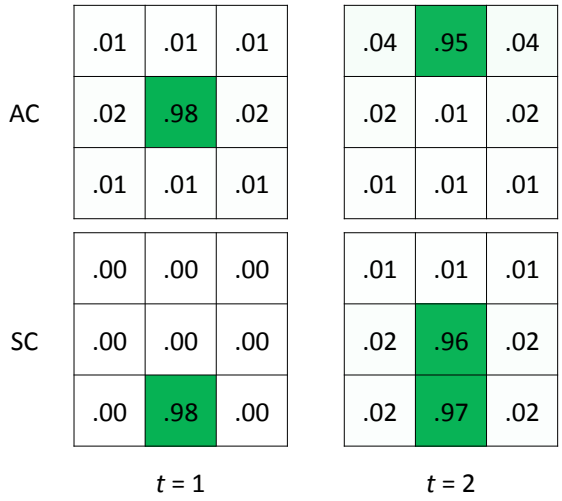

Figure 6: `straight-growth`, `seldom-sprout`. This is the most straightforward setting where the blood vessel grows one step at a time towards north.

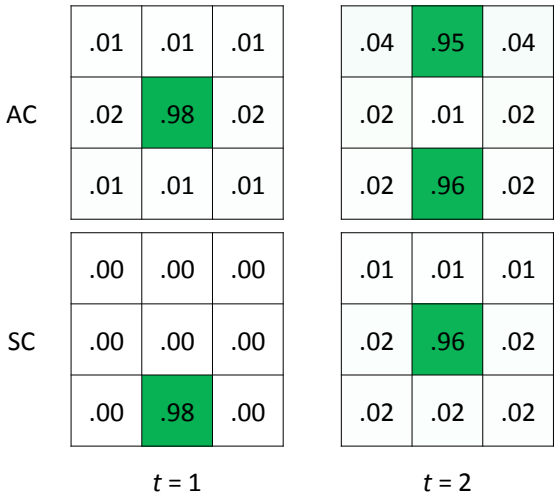

Figure 7: `straight-growth`, `always-sprout`. The blood vessel grows towards north. A location that is a `Stalk Cell` at time $t = 1$ ($L_{x=1,y=0}$) becomes `Active Cell` at time $t = 2$.

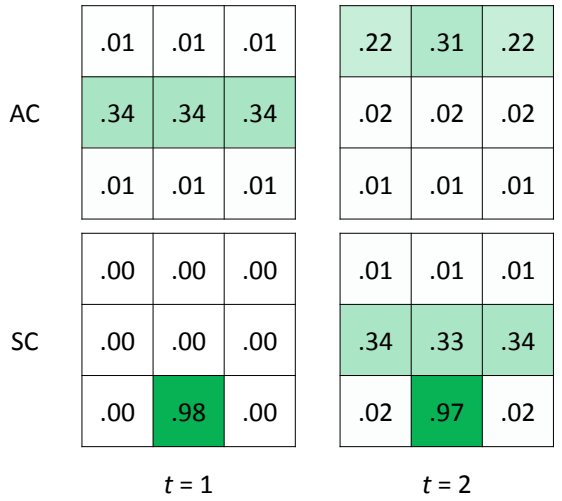

Figure 8: `uniform-growth`, `seldom-sprout`. The blood vessel has equal probability to grow in all three directions. A `Stalk Cell` at time t will most likely remain as `Stalk Cell` at $t + 1$.

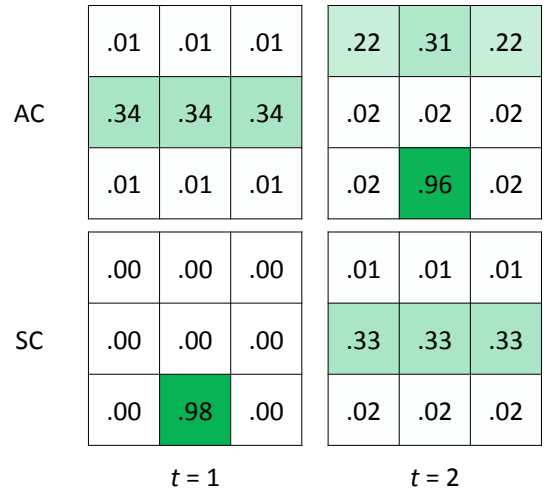

Figure 9: `uniform-growth`, `always-sprout`. The blood vessel has equal probability to grow in all three directions. A `Stalk Cell` will most likely become `Active Cell` in the next time slice.

probability of growing towards NW, N, and NE. In the `seldom-sprout` case (Figure 8), the `Active Cell` at $t = 0$ turned into a `Stalk Cell` at time $t = 1$ and remained a `Stalk Cell` at time $t = 2$. The `Active Cell`, unlike the `straight-growth` case, has equal probability of moving in all three directions. In the last time step, the middle of the top row has higher probability (.31) than the sides (.22) simply because the middle location can be reached from more locations compared to the side locations. The `always-sprout` case (Figure 9) is similar except a `Stalk Cell` at $t = 1$ becomes an `Active Cell` at $t = 2$.

These toy experiments provide insights into how the process typically works. Next, we present results for the 9×9 grid.

4.2 Summary Results for 9×9

Similar to the 3×3 grid, we provide evidence for $t = 0$ case and compute probabilities for the remaining eight time slices. In the initial configuration, the middle

Figure 10: AC and SC probabilities for the 9×9 grid at the last time slice (t=8) for `straight-growth`. Left: `seldom-sprout`. Right: `always-sprout`. On the right, it is apparent that the `Stalk Cells` and `Active Cells` alternate.

of the bottom row is set as an `Active Cell` and the remaining locations are set as `Empty`. Due to space limitations, we present results for only the last time slice, $t = 8$. The `straight-growth` case is shown in Figure 10 and the `uniform-growth` case is shown in Figure 11.

In the `straight-growth seldom-sprout` case (the left side of Figure 10), we see a straight blood vessel for the middle of the grid, where every cell of the blood vessel except the tip is a `Stalk Cell` and the tip is an `Active Cell`, as expected. In the `always-sprout` case (the right side of Figure 10), the `Stalk Cells` and `Active Cells` alternate, again as expected.

In the `uniform-growth seldom-sprout` case (the left side of Figure 11), the blood vessel can be anywhere on the grid, except, as expected, the middle locations have higher probability. In the `always-sprout` case (the right side of Figure 11), the `Stalk Cells` and `Active Cells` alternate, as expected. Additionally, the probabilities for locations being a blood vessel (either Stalk to Active) are higher in the `always-sprout` case compared to the `seldom-sprout` case, again as expected.

The results so far have been nothing surprising, but only confirming our expectations. The value of the DBNs, however, lies at their capability to reason with spatial and temporal uncertainty as well as their potential for future directions. We discuss one of the

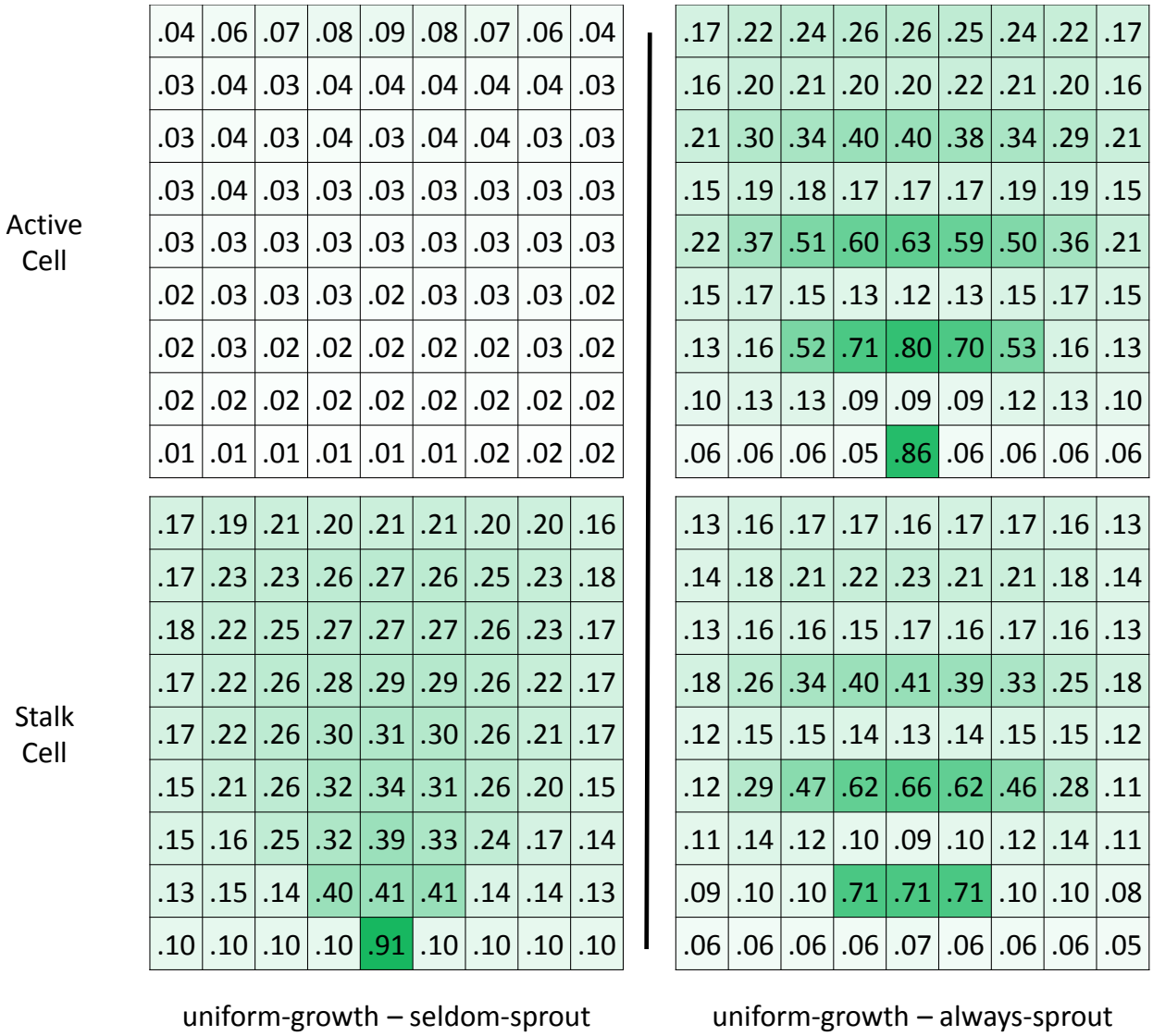

Figure 11: AC and SC probabilities for the 9×9 grid at the last time slice (t=8) for `uniform-growth`. Left: `seldom-sprout`. Right: `always-sprout`. In both cases, the blood vessel can grow uniformly in each direction and the middle locations have higher probability of having a blood vessel simply because they can be reached from multiple locations. In the `always-sprout` case, `Stalk Cells` and `Active Cells` alternate.

future directions here supplemented with some preliminary results, and discuss more future directions in Section 6.

4.3 Quantifying Uncertainty

Given an initial condition, $\mathcal{L}^0$, the tissue engineers are interested in the final status of the tissue, $\mathcal{L}^T$, where T denotes the final step of the experiment. Because real-world experiment take a long time, mostly weeks, they would like to be able to stop an experiment at time $t < T$ and still be able to reason about time T. Therefore, they are interested in the following question: *given an initial condition $\mathcal{L}^0$, if we stop the experiment at time t, what is the uncertainty over $\mathcal{L}^T$?* More practically: *when is the earliest time we can stop an experiment so that the uncertainty over the last time slice is below a pre-specified target σ?*. It is important to note that when an experiment is stopped, the researchers dissect the tissue to analyze its properties, such as vascularization, and hence the experiment cannot continue beyond that point.

Given an uncertainty measure, this question can be formulated rather straightforwardly using DBNs. Let $UNC\left(P\left(\mathcal{L}^T | l^0, l^t\right)\right)$ denote the uncertainty over the predictions over the last time slice, given the initial condition $\mathcal{L}^0 = l^0$ and the status of the experiment at

time t, $\mathcal{L}^t = l^t$. Then, we simply need to find

$$\underset{t<T}{\operatorname{argmin}} UNC\left(P\left(\mathcal{L}^T | l^0, l^t\right)\right) < \sigma \tag{1}$$

Obviously, even though we know the initial conditions l^0, we do not know the status of the experiment at time $t > 0$ unless we stop the experiment. Therefore, we need to take an expectation over all possible outcomes at time t:

$$\underset{t<T}{\operatorname{argmin}} \sum_{l^t} P\left(\mathcal{L}^t = l^t | l^0\right) UNC\left(P\left(\mathcal{L}^T | l^0, l^t\right)\right) < \sigma \tag{2}$$

where the subscript l^t in the summation ranges over all possible configurations of $\mathcal{L}^t$.

Unfortunately the number of all possible configurations for an $n \times n$ grid is $3^{n \times n}$, which is clearly intractable to solve. We leave a more systematic solution for future direction and present results for the case where the summation is replaced with the most probable $l^t | l^0$. For the UNC measure, there are a number of possibilities, including the entropy. We present results where we compute the conditional error of the most probable blood vessel path. That is, for the most-likely blood vessel path, we sum $1 - P(SC|l^t, l^0)$ for the body of the vessel and add $1 - P(AC|l^t, l^0)$ for the tip of the blood vessel.

We experimented with the 9×9 grid and we set the sprout possibility to $\gamma = 0.01$ so that the most probably path does not have any branches. We present the uncertainty values for `straight-growth` and `uniform-growth` patterns in Figure 12. The x axis represents the time we would stop the experiment and the y axis plots the uncertainty. As expected, the uncertainty is much higher for the `uniform-growth` case and that uncertainty goes down for both growth patterns as we provide evidence for later time steps.

We scratched only the surface of this important problem, leaving many interesting research problems for future work, some of which are discussed in Section 6.

5 RELATED WORK

Tissue engineering experiments typically are performed in-vivo usually on mice and in-vitro in glass on lab. Researchers experiment with various settings including the porosity of the scaffold that the tissue is expected to hold on to, the VEGF distribution, and initial blood vessel sprout locations [24, 13, 16, 17].

On the computational side, various researchers have used agent-based modeling to simulate the tissue engineering process [1, 19, 3, 2, 9]. In these simulations, stem cells, tissue cells, and blood cells are modeled as agents and are provided rules that are often elicited from experts. These simulations allow researchers to experiment with a varying number of parameters, without having to perform in-vivo or in-vitro experiments. Some of the parameter settings that produce promising results are then tried in the lab. Based on the results obtained in the lab, the rules for the agents are updated and thus there is often a continuous feedback loop between the simulations and experiments.

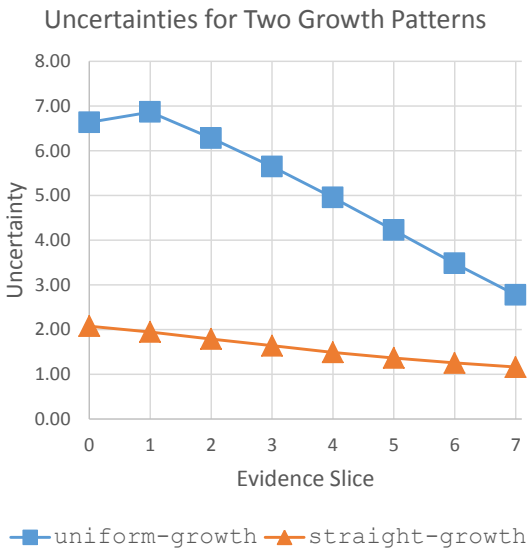

Figure 12: Uncertainties for two growth patterns. As expected, the `straight-growth` pattern is more predictable than the `uniform-growth` pattern. Additionally, providing evidence for later time slices results in lower uncertainties in the last time slice.

Our DBN modeling is a complementary approach to the lab experiments and computational simulations. Because the whole process is inherently stochastic, obtaining the average behavior through experiments and simulations require many trials whereas DBNs provide a systematic, transparent, and modular mechanism to reason with uncertainty.

DBNs have been previously used for many practical applications. Examples include managing water resources [8], modeling environmental problems [23], driverless cars [14], gene regulatory networks [20, 22, 15], figure tracking [21], ranking [10], and speech recognition [25] to name a few. To the best of our knowledge, ours is the first probabilistic graphical model approach for modeling the tissue engineering process.

6 CURRENT LIMITATIONS AND FUTURE DIRECTIONS

There are two lines of work that we would like to pursue in the future. The first type is enriching the model, lifting some of the assumptions we made. The second type of work is a new line of research that we refer to as active inference, which we will describe shortly.

We made a series of simplifying assumptions in our current DBN model. One such assumption is that the tissue space is 2D, whereas in reality it is obviously 3D. The 2D assumption allowed us to work with much fewer random variables. Additionally, in 2D, the number of parents for a variable is four whereas in 3D, the number of parents is ten (itself in the previous time slice and nine locations under it). It is rather straightforward to move from 2D to 3D from a representation perspective. However, scalability both in terms of memory and computational time is a challenge.

Another assumption we made is that the gradient of the VEGF is fixed throughout the grid. That is, we assumed the λ and the γ values are fixed across the grid. In reality, however, the growth factor is expected to have steeper gradient when it is closer to the source of the distressed tissue cell and it is expected to be more uniform as we get further away from the distressed cell. Our simplifying assumption can be easily lifted by providing a growth factor distribution across the grid and then translating it into the necessary λ and γ parameters.

A limitation that is harder to address is scalability. In our experiment section (Section 4), we experimented with 3×3 and 9×9 grids. These were trivial to experiment with. In reality, however, we need to deal with thousands if not millions of random variables over a much longer period of time. This will raise scalability issues both in terms of memory and in terms of computation time. Lifted inference [7] can be used to address some of these challenges.

Another line of research is to formulate and run active inference for dynamic Bayesian networks [6, 5, 4, 12, 11]. Active inference is interested in the following question: *if we are given the opportunity to gather evidence to condition on but gathering evidence is costly, which variables and what time frames are the most cost-effective ones to condition on?*. We discussed the initial formulation of active inference and preliminary results in Section 4.3. However, many questions and challenges remain to be addressed. For example, given a target uncertainty threshold σ, how can we *efficiently* find the smallest time t, where $UNC(P(\mathcal{L}^T|l^0, l^t) < \sigma$, without searching all possible t values?

7 CONCLUSIONS

We presented a dynamic Bayesian network model for vascularization in engineered tissues. This DBN enables i) spatial and temporal reasoning for understanding of vascularization, ii) formulation and investigation of various parameter settings for vascularization, and iii) formulation of uncertainty and active information gathering to minimize uncertainty. We presented initial results that provide insights in to the vascularization process. Though the DBN model currently represents an oversimplification of the reality, it is the first and hence novel application of DBNs to vascularization. As such, it avails itself to many interesting research challenges and opportunities.

Acknowledgments

This material is based upon work supported by the National Science Foundation under grant no. IIS-1125412. We thank Ali Cinar, Judith Zawojewski, Eric Brey, Hamidreza Mehdizadeh, and Elif Bayrak for providing information and insights on tissue engineering.

References

[1] Arsun Artel, Hamidreza Mehdizadeh, Yu-Chieh Chiu, Eric M. Brey, and Ali Cinar. An agent-based model for the investigation of neovascularization within porous scaffolds. *Tissue Engineering Part A*, 17(17-18):2133–2141, 2011.

[2] Alexander M. Bailey, Bryan C. Thorne, and Shayn M. Peirce. Multi-cell agent-based simulation of the microvasculature to study the dynamics of circulating inflammatory cell trafficking. *The Journal of the Biomedical Engineering Society*, 35(6):916 – 936, 2007.

[3] Katie Bentley, Holger Gerhardt, and Paul A. Bates. Agent-based simulation of notch-mediated tip cell selection in angiogenic sprout initialisation. *Journal of Theoretical Biology*, 250(1):25 – 36, 2008.

[4] Mustafa Bilgic and Lise Getoor. Effective label acquisition for collective classification. In *ACM SIGKDD International Conference on Knowledge Discovery and Data Mining*, pages 43–51, 2008.

[5] Mustafa Bilgic and Lise Getoor. Reflect and correct: A misclassification prediction approach to active inference. *ACM Transactions on Knowledge Discovery from Data*, 3(4):1–32, November 2009.

[6] Mustafa Bilgic and Lise Getoor. Active inference for collective classification. In *Twenty-Fourth*

Conference on Artificial Intelligence (AAAI NECTAR Track), pages 1652–1655, 2010.

[7] Rodrigo de Salvo Braz, Eyal Amir, and Dan Roth. Lifted first-order probabilistic inference. In *Proceedings of IJCAI-05, 19th International Joint Conference on Artificial Intelligence*, 2005.

[8] J. Bromley, N. A. Jackson, O. J. Clymer, A. M. Giacomello, and F. V. Jensen. The use of Hugin to develop Bayesian networks as an aid to integrated water resource planning. *Environmental Modelling & Software*, 20(2):231–242, 2005.

[9] Damien P. Byrne, Damien Lacroix, Josep A. Planell, Daniel J. Kelly, and Patrick J. Prendergast. Simulation of tissue differentiation in a scaffold as a function of porosity, young's modulus and dissolution rate: Application of mechanobiological models in tissue engineering. *Biomaterials*, 28(36):5544 – 5554, 2007.

[10] Olivier Chapelle and Ya Zhang. A dynamic Bayesian network click model for web search ranking. In *Proceedings of the 18th International Conference on World Wide Web*, WWW '09, pages 1–10. ACM, 2009. ISBN 978-1-60558-487-4.

[11] Daozheng Chen, Mustafa Bilgic, Lise Getoor, and David Jacobs. Dynamic processing allocation in video. *IEEE Transactions on Pattern Analysis and Machine Intelligence*, 33:2174–2187, 2011.

[12] Daozheng Chen, Mustafa Bilgic, Lise Getoor, David Jacobs, Lilyana Mihalkova, and Tom Yeh. Active inference for retrieval in camera networks. In *Workshop on Person Oriented Vision*, 2011.

[13] Yu-Chieh Chiu, Sevi Kocagoz, Jeffery C Larson, and Eric M Brey. Evaluation of physical and mechanical properties of porous poly (ethylene glycol)-co-(l-lactic acid) hydrogels during degradation. *PLoS One*, 8:4, 2013.

[14] J. Forbes, T. Huang, K. Kanazawa, and S. Russell. The BATmobile: Towards a Bayesian automated taxi. In *IJCAI*, volume 95, 1995.

[15] Dirk Husmeier. Sensitivity and specificity of inferring genetic regulatory interactions from microarray experiments with dynamic Bayesian networks. *Bioinformatics*, 19(17):2271–2282, 2003.

[16] B. Jiang, B. Akar, T.M. Waller, J.C. Larson, A.A. Appel, and E.M. Brey. Design of a composite biomaterial system for tissue engineering applications. *Acta Biomaterialia*, 2013.

[17] Bin Jiang, Thomas M Waller, Jeffery C Larson, Alyssa A Appel, and Eric M Brey. Fibrin-loaded porous poly(ethylene glycol) hydrogels as scaffold materials for vascularized tissue formation. *Tissue engineering. Part A*, 19:224–234, 2013.

[18] R Langer and JP Vacanti. Tissue engineering. *Science*, 260(5110):920–926, 1993.

[19] Hamidreza Mehdizadeh, Sami Sumo, Elif S. Bayrak, Eric M. Brey, and Ali Cinar. Three-dimensional modeling of angiogenesis in porous biomaterial scaffolds. *Biomaterials*, 34(12):2875–2887, 2013.

[20] Zou Min and Suzanne D. Conzen. A new dynamic Bayesian network (DBN) approach for identifying gene regulatory networks from time course microarray data. *Bioinformatics*, 21(1):71–79, 2005.

[21] Vladimir Pavlovic, James M. Rehg, Tat-Jen Cham, and Kevin P. Murphy. A dynamic Bayesian network approach to figure tracking using learned dynamic models. In *Computer Vision, 1999. The Proceedings of the Seventh IEEE International Conference on*, volume 1, pages 94–101 vol.1, 1999.

[22] Bruno-Edouard Perrin, Liva Ralaivola, Aurelien Mazurie, Samuele Bottani, Jacques Mallet, and Florence d'Alche Buc. Gene networks inference using dynamic Bayesian networks. *Bioinformatics*, 19(suppl 2):ii138–ii148, 2003.

[23] L Uusitalo. Advantages and challenges of Bayesian networks in environmental modelling. *Ecological modelling*, 3(203):312–318, 2007.

[24] Shoufeng Yang, Kah-Fai Leong, Zhaohui Du, and Chee-Kai Chua. The design of scaffolds for use in tissue engineering. part I. traditional factors. *Tissue Engineering*, 7:679–689, 2004.

[25] Geoffrey Zweig and Stuat Russell. Speech recognition with dynamic Bayesian networks. In *AAAI-98 Proceedings*, 1998.